Eur. Phys. J. D **62**, 91–102 (2011)
DOI: 10.1140/epjd/e2010-00268-3

THE EUROPEAN PHYSICAL JOURNAL D

Regular Article

Carbon monoxide oxidation on Iridium(111) surfaces driven by strongly colored noise*

J. Cisternas[1,a], R. Lecaros[2], and S. Wehner[3]

[1] Complex Systems Group, College of Engineering and Applied Sciences, Universidad de los Andes, Av. San Carlos de Apoquindo 2200, 762011 Santiago, Chile
[2] Department of Mathematical Engineering, Universidad de Chile, Av. Blanco Encalada 2120, Santiago, Chile
[3] Institut für Integrierte Naturwissenschaften-Physik, Universität Koblenz-Landau, Universitätstraße 1, 56070 Koblenz, Germany

Received 15 May 2010 / Received in final form 3 August 2010
Published online 5 November 2010 –

Abstract. The influence of external colored noise on the carbon monoxide oxidation on Iridium(111) surfaces is examined. The noise is introduced in the reaction by randomly varying the composition of the gas flow that keeps the reaction going on. Colored noise is studied using two models: a simple discrete time Markov chain, and the Ornstein-Uhlenbeck process. We compute the probability distribution and transition times, for medium and large correlation time of the noise. These results extend previous analyses that have been limited to small correlation times and the presence of a slow manifold, both assumptions that are not supported by experiments. As we will see, the correlation and intensity of the noise leads to qualitative changes in the stochastic behavior of the system.

1 Introduction

Surface reactions on crystals of the Platinum group have attracted a good deal of scientific interest during the last decades from the nonlinear science community. In addition to providing models for more complex processes used in industry, some surface reactions exhibit genuine nonlinear behaviors, for instance coexistence of stable states, limit cycles, spatio-temporal patterns, and chaotic dynamics [1–5].

The presence of noise can change the deterministic picture. The effects of internal and external noise on surface reactions have also been addressed, both in theory and in experiments [6–12].

The catalytic oxidation of CO on Ir(111) (described in [5]) provides a model system where the effect of internal noise can be neglected, and external noise can be introduced in a well controlled manner, either by changing the temperature or by changing the composition of the feed gas that flows into the vacuum chamber where the crystal is located. For both methods, random variations can not be arbitrarily fast but are conditioned by how fast the experimental setup can react to changes in the control signals.

In [11,13] the effects induced by Gaussian white noise are studied, using numerical and analytical treatments based on dimensionality reductions. External colored noise imposed on CO oxidation was used in [14], a work that also assessed the effects of non-Gaussianity from the numerical point of view. In [15] we used weakly correlated noise, using the following approximate theories: standard small correlation approximation [16], wideband perturbation expansion [17], and unified colored noise approximation [18]. These theories assume small autocorrelation for the noise but break down when applied to the bistable system under consideration with finite correlation time. Some of these methods can only be used for one-dimensional systems so one must assume there is a slow-manifold where most of the dynamics take place.

In this article our goal is to find approximate solutions to the probability distribution and transition times for medium and large correlation times, with an emphasis on genuine colored-noise effects such as qualitative changes in the probability distribution shape. Noise-induced transitions have already been found and analyzed in a variety of systems. For instance (among many works in the literature) in [17] several cases of monomodal-bimodal-trimodal transitions are observed, as noise intensity or autocorrelation are varied. In ([19] Sect. 3.1.4) a nonlinear oscillator is studied, that in the presence of noise, changes oscillations for switchings between two states. In ([20] Sect. A.3) the authors consider a Ginzburg-Landau type potential that also shows qualitative changes when colored noise is added.

Most of the references in the previous paragraph take advantage of the low dimensionality of the systems under study or particular symmetries. Here we want to study a

* It is a great pleasure to dedicate this work to Prof. Pierre Coullet on the occasion of his 60th birthday.

[a] e-mail: jecisternas@miuandes.cl

specific bistable stochastic problem under colored noise, while trying to keep the discussion as general as possible.

The structure of this work is the following: Section 2 describes the reaction model, Section 3 uses a simple discrete Markov chain to analyze the limit of large correlation time, Section 4 proposes a Ornstein-Uhlenbeck process that captures the medium correlation time and leads to a Fokker-Planck equation, Section 5 implements the Fokker-Planck equations using the finite element method. Finally in Section 6, we conclude by discussing our results.

2 The reaction model

The reaction mechanism of the catalytic CO oxidation on Platinum group metal surfaces:

$$2\ \mathrm{CO} + \mathrm{O_2}\ \rightarrow\ 2\ \mathrm{CO_2},$$

is well established to be the Langmuir-Hinshelwood mechanism, which was shown in 1978 by Engel and Ertl to be the mechanism for catalytic surface reactions [21,22]. It consists of a sequence of three steps:

1. Adsorption of the first reactant:
$$\mathrm{CO(gas)} \rightarrow \mathrm{CO(ad)}$$
2. Adsorption of the second reactant:
$$\mathrm{O_2(gas)} \rightarrow \mathrm{O(ad)} + \mathrm{O(ad)}$$
3. Reaction between adsorbed particles and desorption of the product:
$$\mathrm{O(ad)} + \mathrm{CO(ad)} \rightarrow \mathrm{CO_2(gas)}$$
Here (gas) and (ad) mean gaseous and adsorbed phase respectively.

The kinetics of the chemical processes involved in the reaction can be written as a set of partial differential equations that describe the evolution of the surface concentration of oxygen n_O and carbon monoxide n_CO:

$$\begin{aligned}\frac{\partial n_\mathrm{CO}}{\partial t} &= d_\mathrm{CO}\nabla^2 n_\mathrm{CO} + Y\Phi_\mathrm{total}s_\mathrm{CO}\left(\frac{n_\mathrm{empty}}{n_\mathrm{Ir}}\right)\\ &\quad - n_\mathrm{CO}\nu_\mathrm{deso}\exp(-E_\mathrm{deso}/kT)\\ &\quad - n_\mathrm{CO}n_\mathrm{O}\nu_\mathrm{rea}\exp(-E_\mathrm{rea}/kT), \qquad (1)\\ \frac{\partial n_\mathrm{O}}{\partial t} &= d_\mathrm{O}\nabla^2 n_\mathrm{O} + 2(1-Y)\Phi_\mathrm{total}s_\mathrm{O}\left(\frac{n_\mathrm{empty}}{n_\mathrm{Ir}}\right)^3\\ &\quad - n_\mathrm{CO}n_\mathrm{O}\nu_\mathrm{rea}\exp(-E_\mathrm{rea}/kT). \qquad (2)\end{aligned}$$

The available number of sites on the iridium surface is constant:

$$n_\mathrm{Ir} = n_\mathrm{empty} + n_\mathrm{CO} + n_\mathrm{O}. \qquad (3)$$

The parameter Y is the molar fraction of CO in the total feed gas flux Φ_total. In the first term of equation (1), the effective number of CO molecules in the gas that reaches the surface (per unit of time) is $Y\Phi_\mathrm{total}$. For $\mathrm{O_2}$ molecules the effective number is $(1-Y)\Phi_\mathrm{total}$. The probability for each CO molecule to get adsorbed is $s_\mathrm{CO}(n_\mathrm{empty}/n_\mathrm{Ir})$. For the CO desorption, the number of molecules on the surface that can desorb is n_CO, and the rate is ν_deso times the activation factor. The third term in equation (1) and the second one in equation (2) consider the reaction that takes place when an adsorbed molecule of CO meets an adsorbed O. The sticking coefficients $s_\mathrm{CO}, s_\mathrm{O}$ are nondimensional factors that can be interpreted as probabilities. For simplification s_CO was taken to unity and the ratio $s_\mathrm{O}/s_\mathrm{CO}$ was adjusted from experimental data.

In this work we will focus on stochastic behaviours that can be explained without using macroscopic diffusion. As in [6], we will assume from now on that n_CO and n_O depend on time only.

Defining the following nondimensional quantities:

$$u \stackrel{\mathrm{def}}{=} n_\mathrm{CO}/n_\mathrm{Ir},\ v \stackrel{\mathrm{def}}{=} n_\mathrm{O}/n_\mathrm{Ir},$$

the *ordinary* differential equations (1)–(3) can be scaled:

$$\frac{du}{dt} = \alpha Y(1-u-v) - \beta u - \gamma uv, \qquad (4)$$

$$\frac{dv}{dt} = \delta(1-Y)(1-u-v)^3 - \gamma uv, \qquad (5)$$

where we have intentionally left the parameter Y free so it can be used as a source of random variations. Representative values for the four parameters for a temperature $T = 500$ K are (in units of 1/s): $\alpha = 0.878205, \beta = 0.023692, \gamma = 6.640593, \delta = 0.193205$. These values are used without modification in the rest of the article.

Depending on the value of the parameter Y, the reaction has one stable steady state, or two stable and one unstable steady states. As depicted in Figure 1, when the parameter Y is varied, these two stable states define two separate branches that we call upper rate (UR) and lower rate (LR). The reaction rate i.e. the $\mathrm{CO_2}$ production formation corresponds to the partial pressure of 44 amu, measured by a quadrupole mass spectrometer, and is proportional to:

$$n_\mathrm{CO}n_\mathrm{O}\nu_\mathrm{rea}\exp(-E_\mathrm{rea}/kT).$$

For practical purposes we consider the nondimensional rate $z \stackrel{\mathrm{def}}{=} uv$.

It has been shown experimentally that the coexistence of the two branches defines an interval between Y_ℓ and Y_h where the system is bistable. Inside the window, there is a hysteretic loop: as the control parameter Y is slowly increased beyond Y_ℓ, the reaction rate lies along the UR branch until it disappears at Y_h, then switches to LR. As Y is decreased below Y_h, the reaction rate sticks to LR until the branch turns around at Y_ℓ and the reaction rate jumps to UR. As indicated in Figure 1, the model defined by equations (4), (5) captures these behaviors.

The existence and stability of steady states can be understood in phase plane (u, v), where fixed points move and annihilate as the parameter Y is varied beyond $Y_\ell \approx 0.073$ or below $Y_h \approx 0.1215$ (these values correspond to the model). All the dynamics take place inside a triangle:

$$\Omega_2 \stackrel{\mathrm{def}}{=} \{(u,v) \mid 0 \le u \le 1, 0 \le v \le 1, u+v \le 1\},$$

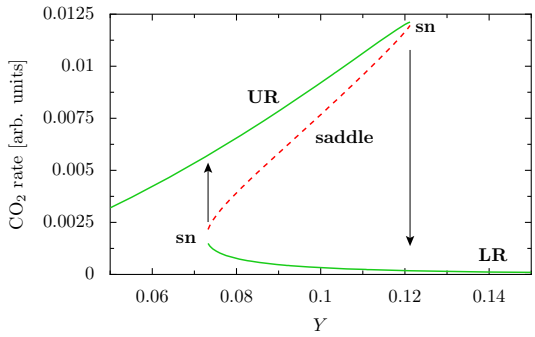

Fig. 1. (Color online) Fixed points of equations. (4), (5). The stable branches define the upper rate (UR) and lower rate (LR) stationary solutions that define the hysteretic loop. The unstable branch (made up of saddle points) is not observable but plays an important role in the stochastic dynamics. The turning points of the curve define two saddle-node bifurcations (sn).

regardless of the value of Y. The restrictions $u \geq 0$ and $v \geq 0$ come from the definition of u, v as coverages of molecules on the surface. The restriction $u + v \leq 1$ comes from the finite number of adsorption sites in the lattice. It can be verified that the vectorfield $\dot{u}\hat{\mathbf{u}} + \dot{v}\hat{\mathbf{v}}$ defined by the differential equations (4), (5) along the three edges of the domain always points inwards: meaning that $\partial\Omega_2$ is an entrance boundary.

2.1 External noise

The preferred experimental method for adding external random perturbations is by controlling the CO fraction of gas flux $Y(t) = \Phi_{\mathrm{CO}}/\Phi_{\mathrm{total}}$ in a random manner, holding its value constant for fixed periods of time. For some Y_0 and ΔY $(0 \leq Y_0 \leq 1)$, the value of $Y(t)$ is updated every τ_n seconds following the distribution:

$$p(Y) = \begin{cases} \mathcal{N} \exp\left(-\frac{1}{2}\left(\frac{Y-Y_0}{\Delta Y/2}\right)^2\right) & \text{if } |Y - Y_0| \leq \Delta Y, \\ 0 & \text{otherwise.} \end{cases} \tag{6}$$

The standard deviation of Y is $\Delta Y_{\mathrm{eff}}/2$ with $\Delta Y_{\mathrm{eff}} \stackrel{\mathrm{def}}{=} \kappa \Delta Y$ where:

$$\kappa^2 = \frac{\int_{-2}^{2} x^2 \exp(-x^2/2)\, dx}{\int_{-2}^{2} \exp(-x^2/2)\, dx} \approx 0.8796.$$

The smallest value of τ_n that can be achieved in the current experimental setting is around one second. This limitation comes from the finite time required for readjusting the mass flow controller and the time required for the gas to reach the chamber through a capillary. The longest value of τ_n is around 100 s.

Defining:

$$y(t) \stackrel{\mathrm{def}}{=} Y(t) - Y_0$$

one can verify that:

$$\langle y(t) \rangle = 0,$$

and

$$\langle y(s) y(t) \rangle = \begin{cases} \frac{D}{\tau_n}\left(1 - \frac{|t-s|}{\tau_n}\right) & \text{if } |s-t| < \tau_n, \\ 0 & \text{otherwise,} \end{cases}$$

where the effective strength of the noise:

$$D \stackrel{\mathrm{def}}{=} \frac{\tau_n}{2}\left(\frac{\Delta Y_{\mathrm{eff}}}{2}\right)^2. \tag{7}$$

This piecewise-constant noise has an intrinsic correlation time:

$$\tau \stackrel{\mathrm{def}}{=} \frac{\int_0^\infty \langle y(t) y(0) \rangle dt}{\langle y^2 \rangle} = \frac{\tau_n}{2}. \tag{8}$$

This finite correlation time invalidates the use of white noise and raises the question of whether it would change the stationary or transient behavior of the stochastic system. As discussed in [15], colored noise can have a direct effect on the shape of the probability distribution, leading to qualitative changes that are the main motivation behind this work.

Figure 2 displays a summary of three experiments obtained with photoelectron emission microscopy (PEEM) that roughly speaking represents LR (CO-covered) with gray and UR (O-covered) with black. For these small intensities of the noise, small UR islands are created at random points on the surface. As time advances, the islands grow until covering the whole surface. In the next section we will show that for higher values of ΔY, it was possible to observe transitions back and forth between LR and UR states.

A full study of the influence of noise in the bistable system should consider all combinations of values of τ_n and ΔY, for $Y_0 \in (Y_\ell, Y_h)$. As indicated in [15], several approximations have been devised to study small τ behavior, but either break down or give extremely inaccurate results for finite correlation times.

3 Quasi-static approach

In our study of nonzero correlation time for the external noise, an extreme situation would be to consider a very large value of τ_n, for instance $\tau_n \gg 10$ s, which is much larger than any characteristic time scales of the deterministic dynamics explained by equations (4), (5).

In this limit, the system can be effectively considered as residing at one of the stable fixed points compatible with the current value of $Y(t)$. When there is only one fixed point this reasoning leads to the *switching-curve approximation* for the steady state distribution (see for instance [16]):

$$W_{\mathrm{rate}}(z) = p(Y)\left(\frac{dz}{dY}\right)^{-1}$$

with z the reaction rate of the fixed point of deterministic dynamics equations (4), (5) that gives the distribution along the branch of fixed points.

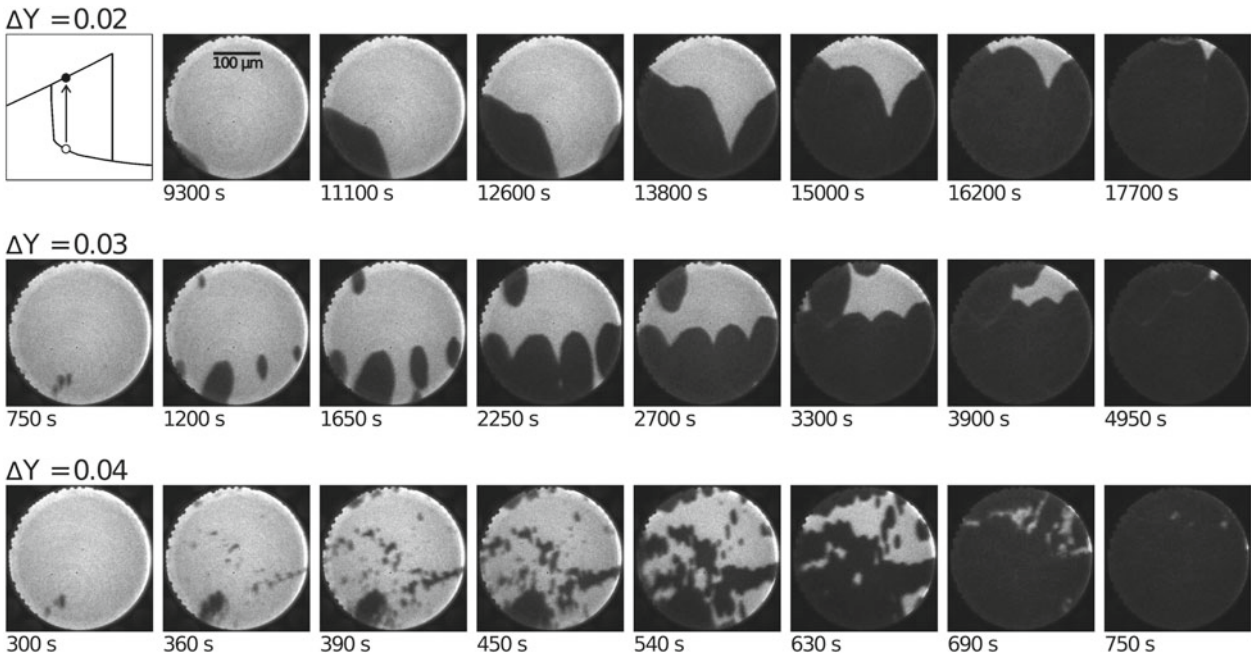

Fig. 2. Three series of PEEM for different noise strengths (top $\Delta Y = 0.02$, middle $\Delta Y = 0.03$, bottom $\Delta Y = 0.04$) superposed on $Y_0 = 0.11$, as depicted on icon at upper-left corner. The time below each picture specifies the time that has passed since the experiment started in LR. Growth of oxygen islands (dark) on an initially CO-covered surface (gray) is recorded. The number of islands and therefore the transient time depends on Y noise strength. The field of view is 310 μm (black bar in left top picture is 100 μm). Reprinted with permission from Wehner et al., "Influence of the Substrate on the Pattern Formation of a Surface Reaction", AIP Conference Proceedings 913: Nonequilibrium Statistical Mechanics and Nonlinear Physics. Copyright 2007, American Institute of Physics.

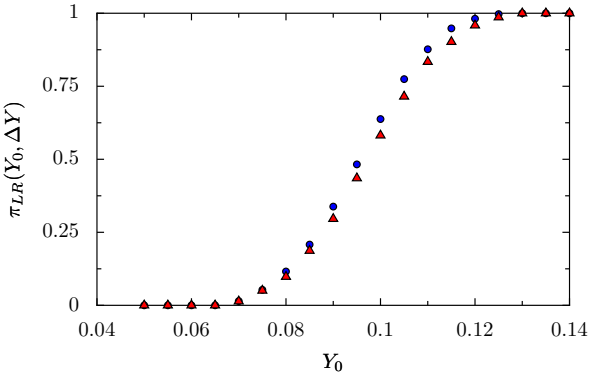

Fig. 3. (Color online) Steady state probability of being at the state LR for different values of Y_0 and fixed ΔY. Blue circles show numerical simulation for $\tau_n = 500$ s and $\Delta Y = 0.0548$, red triangles show results of quasi-static approach equation (10).

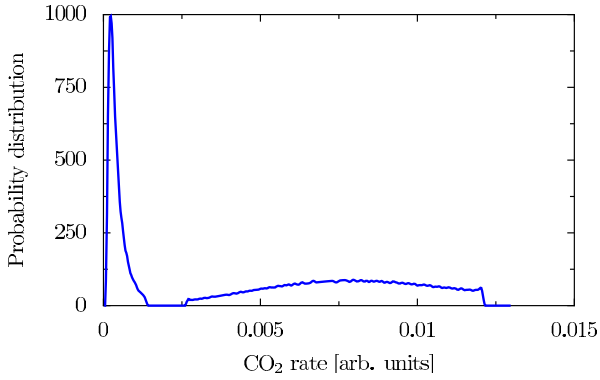

Fig. 4. (Color online) Reaction rate distribution computed using a quasi-static approach equation (11): probability distribution of each branch was weighted using probabilities $\pi_{\rm LR}$ (left) and $\pi_{\rm UR}$ (right). Two distinct peaks reflect the presence of two branches.

But for the *bistable* case there are two branches, and more important than the shape of $p(u)$ is the probability of being at one branch or the other. These probabilities depend on the frequencies of switching events.

For the bistable case one needs to refine the argument and compute the probability of residing at each branch after every time $Y(t_n)$ is updated: $\pi_{\rm UR}(n)$ and $\pi_{\rm LR}(n)$. Jumps from UR to LR are going to take place every time $Y(t) > Y_h$, and jumps from LR to UR every time $Y(t) > Y_\ell$. The following discrete-time Markov chain model describes these transitions:

$$\begin{aligned}\pi_{\rm UR}(n+1) &= \pi_{\rm UR}(n)P(Y < Y_h) + \pi_{\rm LR}(n)P(Y < Y_\ell),\\ \pi_{\rm LR}(n+1) &= \pi_{\rm UR}(n)P(Y > Y_h) + \pi_{\rm LR}(n)P(Y > Y_\ell).\end{aligned} \tag{9}$$

The unique stationary solution can be found right away:

$$\begin{aligned}\pi_{\rm UR} &= \frac{P(Y < Y_\ell)}{P(Y < Y_\ell) + P(Y > Y_h)},\\ \pi_{\rm LR} &= \frac{P(Y > Y_h)}{P(Y < Y_\ell) + P(Y > Y_h)}.\end{aligned} \tag{10}$$

Table 1. Comparison between the expected fraction of the time the system spends around LR in experiments [23] and in the quasi-static model (10). Y_0 reflects the location on the hysteretic range $[Y_\ell, Y_h]$. All quantities are nondimensional. The comparison is meant to be qualitative only, as in each row the Y_0 values were chosen so they correspond to similar locations in the hysteresis loops in the experiment and in the model.

Experiment			Quasi-static model		
Y_0	ΔY	$\pi_{\rm LR}$	Y_0	ΔY	$\pi_{\rm LR}$
0.11	0.10	0.628	0.085	0.10	0.375
0.12	0.12	0.740	0.097	0.12	0.500
0.13	0.10	0.953	0.116	0.10	0.707

Results in Figure 3 show how this simple model can account for some of the trends at large correlation time τ. Weighting the switching curve approximation by the probabilities $\pi_{\rm UR}$ and $\pi_{\rm LR}$ one can compute the distribution of reaction rates in the bistable range. The following formal expression can be used:

$$W_{\rm rate}(z) = \pi_{\rm LR}\, p(Y_{\rm LR}(z))\frac{dY_{\rm LR}}{dz} + \pi_{\rm UR}\, p(Y_{\rm UR}(z))\frac{dY_{\rm UR}}{dz}, \tag{11}$$

where it is understood that if $Y_{\rm LR}$ ($Y_{\rm UR}$) does not exist for a particular value of the rate z, the first (second) term does not contribute. Figure 4 shows two well defined peaks of different heights and widths, constructed using this quasi-static approach.

Probabilities $\pi_{\rm UR}$ and $\pi_{\rm LR}$ can also be contrasted directly to experiments. Figure 5 displays a summary of three experiments obtained with PEEM, showing transitions between UR and LR states. Each spacetime plot shows the reaction rate of a thin segment on the iridium crystal. For these intensities of the noise, transitions take place on the surface more or less simultaneously and are not mediated by growing islands. As Y is increased inside the bistable range, the basin of attraction of the state LR becomes larger and more stable. In Table 1, a qualitative comparison is made between the experiments and the quasi-static model. Although the agreement is not sharp, the model does capture some trends of what is actually happening in experiments.

Using this quasi-static formalism the following question can also be solved: how long does it take for the system to switch from UR to LR (or the other way around)? The question can be translated to the mean residence time in branch UR:

$$T_{\rm UR} = \frac{\tau_n}{P(Y > Y_h)}, \tag{12}$$

that depends on τ_n, Y_0 and ΔY. This linear dependence on correlation time will be examined in the next section using more elaborate methods valid for finite correlation time.

4 Ornstein-Uhlenbeck noise

A most useful choice in the treatment of colored noise is the Ornstein-Uhlenbeck process, which can be tailored to mimic the basic statistical properties of the piecewise-constant noise. Among the references in the literature where such approach has been used we can cite [16,17,19,20,24].

The Ornstein-Uhlenbeck process generates colored noise as an auxiliar degree of freedom $\zeta(t) \in \mathbb{R}$:

$$\dot\zeta = \frac{1}{\tau}\left(-\zeta + \xi\right)$$

where $\xi(t)$ is a white noise process:

$$\langle \xi(t)\rangle = 0,\ \langle \xi(s)\xi(t)\rangle = 2\delta(t-s).$$

The statistics of the colored noise $\zeta(t)$ are:

$$\langle \zeta(t)\rangle = 0,\ \langle \zeta(s)\zeta(t)\rangle = \frac{1}{\tau}\exp(-|t-s|/\tau).$$

For D and τ defined in equations (7), (8), the function $Y(t) = Y_0 + \sqrt{D}\zeta(t)$ has the same correlation time and standard deviation that the piecewise-constant $Y(t)$ used in experiments and defined in equation (6).

Now our system of stochastic differential equations looks like:

$$\dot u = f_u(u,v) + g_u(u,v)\sqrt{D}\zeta \tag{13}$$

$$\dot v = f_v(u,v) + g_v(u,v)\sqrt{D}\zeta \tag{14}$$

$$\dot\zeta = -\frac{1}{\tau}\zeta + \frac{1}{\tau}\xi \tag{15}$$

where the nonlinear functions:

$$\begin{aligned} f_u &\stackrel{\rm def}{=} \alpha Y_0(1-u-v) - \beta u - \gamma uv,\\ f_v &\stackrel{\rm def}{=} \delta(1-Y_0)(1-u-v)^3 - \gamma uv, \end{aligned} \tag{16}$$

and

$$\begin{aligned} g_u &\stackrel{\rm def}{=} \alpha(1-u-v),\\ g_v &\stackrel{\rm def}{=} -\delta(1-u-v)^3, \end{aligned} \tag{17}$$

defined in the three-dimensional domain:

$$\Omega_3 \stackrel{\rm def}{=} \Omega_2 \times \mathbb{R},$$

an infinite cylinder with triangular section.

Notice that the system is driven by the white noise $\xi(t)$ term in the third equation. The system equations (13)–(15) is Markovian, and its associated Fokker-Planck equation for the probability density $W(u,v,\zeta,t)$:

$$\begin{aligned} \partial_t W &= \mathcal{L}W\\ &= -\partial_u\left[(f_u + \sqrt{D}g_u\zeta)W\right] - \partial_v\left[(f_v + \sqrt{D}g_v\zeta)W\right]\\ &\quad + \frac{1}{\tau}\partial_\zeta(\zeta W) + \frac{1}{2\tau^2}\partial_\zeta^2 W. \end{aligned} \tag{18}$$

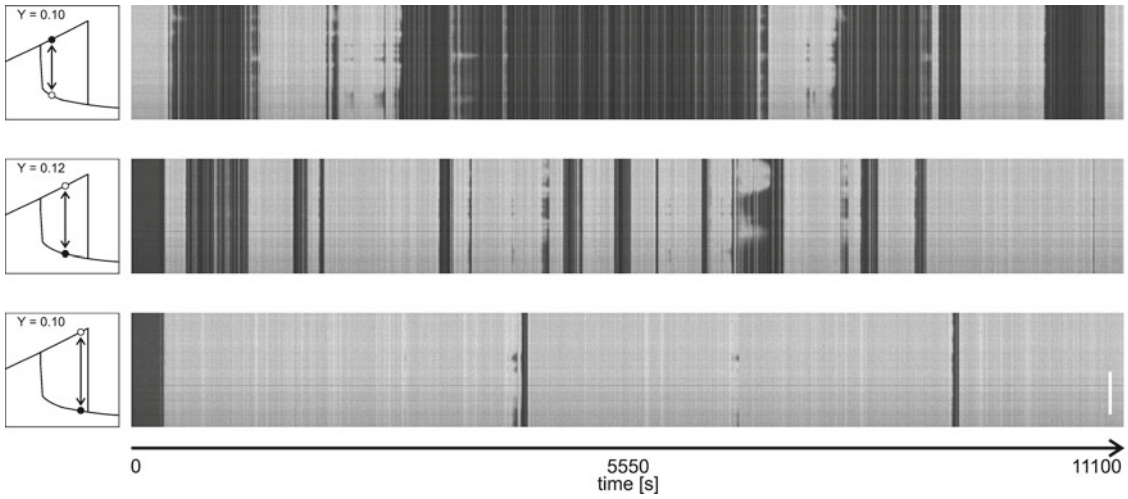

Fig. 5. Space-time representation of a centered 270 μm vertical pixel line covering the period of 11 100 s for three series of PEEM with large Y noise strength. Y position in the hysteresis region for each experiment is shown in the icons on the left side. The white bar at the right of the bottom picture is 100 μm long. The thin vertical black line seen in the middle and bottom images is due to a blind spot of the channelplate used in the PEEM. Reprinted from [23]. Reproduced with permission from World Scientific Publishing Co. Pte. Ltd.

We can recognize terms that come from the deterministic dynamics ($D = 0$), the dynamics of auxiliar variable ζ, and the coupling between them.

There are second derivatives only for variable ζ (diffusion takes place only along the axis of the cylinder). 'Horizontal' motion is purely deterministic. In equation (18) we can see that the limit of zero noise i.e. the Liouville equation, is well defined, because u, v and ζ variables decouple. The limit of large τ corresponds to zero flux in the vertical direction. The limit of small autocorrelation can not be extracted with the same ease.

The total probability must be conserved, thus appropriate boundary conditions should be used (more on this will come later). Integrating in the whole domain:

$$\int_{\Omega_3} W \, du \, dv \, d\zeta = 1$$

implies:

$$\int_{\Omega_3} \partial_t W \, du \, dv \, d\zeta = \int_{\Omega_3} \mathcal{L} W \, du \, dv \, d\zeta = 0$$

for any probability distribution $W(u, v, \zeta, t)$. The previous equation can then be interpreted in the following way: the characteristic function of the domain belongs to the left-nullspace of $\mathcal{L}$, so its right-nullspace also has at least one member, and the Fokker-Planck operator $\mathcal{L}$ has at least one zero eigenvalue.

Defining in the interior of the cylinder Ω_3 the three-dimensional vector field (probability current):

$$\mathbf{F} \stackrel{\text{def}}{=} \left(-f_u W - \sqrt{D} g_u \zeta W\right) \hat{\mathbf{u}} + \left(-f_v W - \sqrt{D} g_v \zeta W\right) \hat{\mathbf{v}} + \left(\frac{1}{\tau} \zeta W + \frac{1}{2\tau^2} \partial_\zeta W\right) \hat{\zeta}, \tag{19}$$

we get an alternative expression of the FPE (18):

$$\partial_t W = \mathcal{L} W = \partial_u F_u + \partial_v F_v + \partial_\zeta F_\zeta. \tag{20}$$

From this last expression and using Green's theorem we obtain:

$$\int_{\Omega_3} \mathcal{L} W \, du \, dv \, d\zeta = \oint_{\partial\Omega_3} \mathbf{F} \cdot \hat{\mathbf{n}} \, ds = 0,$$

which suggests that to guarantee strict conservation of probability we should impose that the boundaries be *reflecting*:

$$\mathbf{F} \cdot \hat{\mathbf{n}} = 0 \quad \text{in} \quad \partial\Omega_3. \tag{21}$$

Boundary conditions can be further simplified using the properties of functions f_u, f_v, g_u, g_v (defined in Eqs. (16), (17)) on $\partial\Omega_3$:

(i) At $u = 0$ $(0 \le v \le 1, \zeta \in \mathbb{R})$:

$$-f_u W - \sqrt{D} g_u \zeta W = 0 \implies W|_{u=0} = 0$$

(ii) At $v = 0$ $(0 \le u \le 1, \zeta \in \mathbb{R})$:

$$-f_v W - \sqrt{D} g_v \zeta W = 0 \implies W|_{v=0} = 0$$

(iii) At $u + v = 1$ $(0 \le u, 0 \le v, \zeta \in \mathbb{R})$:

$$-f_u W - \sqrt{D} g_u \zeta W - f_v W - \sqrt{D} g_v \zeta W = 0 \implies W|_{u+v=1} = 0$$

(iv) At $\zeta = \pm\infty$ $(0 \le v, 0 \le 1, u + v \le 1)$:

$$\left(\frac{1}{\tau} \zeta W + \frac{1}{2\tau^2} \partial_\zeta W\right) = 0 \implies \lim_{\zeta \to \pm\infty} W = 0$$

Exponential decay in ζ could be used.

These boundary conditions enforce that the total probability (inside the cylinder) is conserved.

4.1 Expansion into a complete set

The 3-dim linear PDE (18) can in principle be solved using finite differences. But (following the book of Risken ([25] Sect. 5.3)) it can also be solved using an expansion into a *complete set*:

$$W(u,v,\zeta;t) = \mu\bar{W} = \mu(u,v,\zeta)\sum_{\ell=0}^{\infty}\phi_\ell(u,v,t)\theta_\ell(\zeta). \quad (22)$$

A good selection of functions $\mu(u,v,\zeta)$ and $\theta_\ell(\zeta)$ leads to an economical representation of $\mathcal{L}$ and a method to solve for $\phi_\ell(u,v,t)$ at least approximately. In the following we will use:

$$\mu(\zeta) = \theta_0(\zeta) \stackrel{\text{def}}{=} \left(\frac{\tau}{\pi}\right)^{1/4}\exp(-\tau\zeta^2/2),$$

the square root of the stationary distribution of ζ.

Another way of motivating the approach is the following transformation:

$$\bar{\mathcal{L}} \stackrel{\text{def}}{=} \theta_0^{-1}(\zeta)\mathcal{L}\theta_0(\zeta),$$
$$\bar{W} \stackrel{\text{def}}{=} \theta_0^{-1}(\zeta)W. \quad (23)$$

Naturally if $\bar{W}$ is a solution of $\bar{\mathcal{L}}$ then W will be a solution of $\mathcal{L}$.

Defining *annihilation* and *creation* operators:

$$b \stackrel{\text{def}}{=} \frac{1}{\sqrt{2\tau}}\frac{\partial}{\partial_\zeta} + \frac{\sqrt{2\tau}}{2}\zeta,$$
$$b^\dagger \stackrel{\text{def}}{=} -\frac{1}{\sqrt{2\tau}}\frac{\partial}{\partial_\zeta} + \frac{\sqrt{2\tau}}{2}\zeta, \quad (24)$$

that verify the *bosonic* commutation relation:

$$[b\ , b^\dagger] = 1,$$

and

$$\zeta = \frac{b+b^\dagger}{\sqrt{2\tau}}, \quad \partial_\zeta = \sqrt{\frac{\tau}{2}}(b-b^\dagger).$$

Using these operators, the expression of the Fokker-Planck operator can be simplified:

$$\bar{\mathcal{L}} = (-\partial_u f_u - \partial_v f_v) - \frac{1}{\tau}b^\dagger b - \frac{\sqrt{D}}{\sqrt{8\tau}}(b+b^\dagger)(\partial_u g_u + \partial_v g_v), \quad (25)$$

where the first term involves a deterministic flow, and the second and third terms correspond to noise effects. Notice that operator b (as well as $b^\dagger$) commutes with partial derivatives ∂_u and ∂_v.

The compact representation of equation (25) suggests using Hermite functions[1] $\theta_\ell(\zeta)$:

$$\sqrt{\ell+1}\ \theta_{\ell+1}(\zeta) = b^\dagger\theta_\ell(\zeta), \quad \sqrt{\ell}\ \theta_{\ell-1}(\zeta) = b\ \theta_\ell(\zeta),$$

[1] The functions defined by:

$$\theta_0(\zeta) = \left(\frac{\tau}{\pi}\right)^{1/4}\exp(-\zeta^2\tau/2),\ \sqrt{\ell+1}\ \theta_{\ell+1}(\zeta) = b^\dagger\theta_\ell(\zeta)$$

satisfy

$$\int \theta_m(\zeta)\theta_n(\zeta)\ d\zeta = \delta_{mn}.$$

It can be verified that:

$$\theta_\ell(\zeta) = \frac{H_\ell(\zeta\sqrt{\tau})e^{-\zeta^2\tau/2}}{\sqrt{\ell!\ 2^\ell\sqrt{\pi/\tau}}}$$

where $H_\ell(x)$ are physicist's Hermite polynomials, with leading coefficient 2^ℓ, and

$$\int H_n(x)H_m(x)e^{-x^2}\ dx = n!\ 2^n\sqrt{\pi}\delta_{mn}.$$

One possibility for ϕ_ℓ would be to further expand:

$$\phi_\ell(u,v;t) = \sum_{m,n} c_{m,n,\ell}(t)\phi_{m,n,\ell}(u,v),$$

where $\phi_{m,n,\ell}$ satisfy boundary conditions (21). One could for instance use combinations of sinusoids defined in Ω_2. This expansion would lead to a differential recurrence relation as in [24], that can be solved by the matrix continued fraction (MCF) method presented in [25].

For the specific chemical reaction we are studying, MCF is not effective for several reasons: it is difficult to select functions that verify boundary conditions; the use of harmonic functions may lead to the appearance of regions with negative probability W; and the probability distribution becomes increasingly localized in (u,v) space and a large number of terms would be necessary.

Here we develop a somewhat different method, expanding $\bar{W}$ as a sum over Hermite functions without making any assumptions about (u,v) dependence. This approach is also applicable to the exit time problem developed in Section 4.2.

Replacing the Ansatz (22) in the Fokker-Planck equation (25) and in the boundary conditions, we get a set of *coupled* two-dimensional partial differential equations for $\phi_\ell(u,v,t)$:

$$\partial_t\phi_\ell = -(\partial_u f_u + \partial_v f_v)\phi_\ell - \frac{\ell}{\tau}\phi_\ell - \sqrt{\frac{D}{8\tau}}(\partial_u g_u + \partial_v g_v)\left(\sqrt{\ell+1}\phi_{\ell+1} + \sqrt{\ell}\phi_{\ell-1}\right), \quad \text{in } \Omega_2 \text{ for } \ell = 0,1,2,\ldots \quad (26)$$

Each one of equation (26) has terms that correspond to: deterministic flow (Liouville operator); relaxation (other than $\ell = 0$); and coupling with other layers due to noise.

When D is small all the layers decay and only the first mode $\phi_0(u,v,t)\theta_0(\zeta)$ is relevant, meaning that the variables u, v are decoupled from the noise ζ. Now, when τ is small, there is no easy way to identify first order terms. This is not a small-τ approach and does not try to separate terms associated to D and τ, but as we will show this approach does indeed capture the effects of colored noise.

Relevant expected values can be obtained from:

$$W(u,v,t) = \int_{-\infty}^{\infty} \theta_0(\zeta) \sum_{\ell=0} \phi_\ell(u,v,t)\theta_\ell(\zeta)\, d\zeta = \phi_0(u,v,t).$$

For the initial condition we should assume that at preparation time $t = 0$ the auxiliary variable follows its stationary distribution:

$$W(\zeta,0) = \int_{\Omega_2} W(u,v,\zeta,0)\, du\, dv = \theta_0^2(\zeta),$$

so we can assume:

$$\phi_0(u,v,0) = 2,$$

the inverse of the area of the triangle Ω_2. From the probability distribution one can compute the distribution of the nondimensional reaction rate $z = uv$:

$$W_{\text{rate}}(z,t) = \int_0^1 \phi_0(u, z/u, t)\, du.$$

Each one of equations (26) also looks like a flux:

$$\partial_t \phi_\ell + \frac{\ell}{\tau}\phi_\ell = \nabla \cdot \mathbf{F}_\ell \text{ in } \Omega_2 \tag{27}$$

where ∇ is the divergence operator in (u,v) space and $\mathbf{F}_\ell$ is a set of vectorfields in two-dimensional (u,v) space:

$$\mathbf{F}_\ell \stackrel{\text{def}}{=} \left(-f_u\phi_\ell - \sqrt{\frac{D}{8\tau}}g_u(\sqrt{\ell+1}\phi_{\ell+1} + \sqrt{\ell}\phi_{\ell-1})\right)\hat{\mathbf{u}} + \left(-f_v\phi_\ell - \sqrt{\frac{D}{8\tau}}g_v(\sqrt{\ell+1}\phi_{\ell+1} + \sqrt{\ell}\phi_{\ell-1})\right)\hat{\mathbf{v}} \tag{28}$$

(where each $\mathbf{F}_\ell$ depends on $\phi_{\ell-1}, \phi_\ell, \phi_{\ell+1}$).

For the boundary conditions, equation (21) implies that $\mathbf{F}_\ell \cdot \hat{\mathbf{n}} = 0$ in $\partial\Omega_2$, for $\ell = 0, 1, 2, \ldots$ and we get:

(i) At $u = 0$:

$$-f_u\bar{W} - \sqrt{D}g_u\frac{(b+b^\dagger)}{\sqrt{2\tau}}\bar{W} = 0$$

so

$$-f_u\phi_\ell - \sqrt{\frac{D}{2\tau}}g_u\left(\sqrt{\ell+1}\phi_{\ell+1} + \sqrt{\ell}\phi_{\ell-1}\right) = 0,$$

for $\ell = 0, 1, 2, \ldots$

(ii) At $v = 0$:

$$-f_u\bar{W} - \sqrt{D}g_u\frac{(b+b^\dagger)}{\sqrt{2\tau}}\bar{W} = 0$$

so

$$-f_v\phi_\ell - \sqrt{\frac{D}{2\tau}}g_v\left(\sqrt{\ell+1}\phi_{\ell+1} + \sqrt{\ell}\phi_{\ell-1}\right) = 0,$$

for $\ell = 0, 1, 2, \ldots$

(iii) At $u + v = 1$:

$$-(f_u+f_v)\phi_\ell - \sqrt{\frac{D}{2\tau}}(g_u+g_v)\left(\sqrt{\ell+1}\phi_{\ell+1} + \sqrt{\ell}\phi_{\ell-1}\right) = 0,$$

for $\ell = 0, 1, 2, \ldots$

(iv) The boundary conditions at $\eta = \pm\infty$ are automatically verified, because of the $\exp(-\zeta^2\tau/2)$ factor.

In summary, we can use Dirichlet boundary conditions in all three edges:

$$\phi_\ell = 0 \text{ in } \partial\Omega_2 \text{ for all } \ell = 0, 1, 2, \ldots \tag{29}$$

The evolution problem can be implemented iteratively using the backward Euler method:

$$\frac{\phi_\ell^{m+1} - \phi_\ell^m}{\Delta t} = \nabla \cdot \mathbf{F}_\ell^{m+1} - \frac{\ell}{\tau}\phi_\ell^{m+1}$$

with appropriate initial condition ϕ_ℓ^0 and Dirichlet boundary conditions for ϕ_ℓ^{m+1}.

4.2 First exit time problem

The evolution of stochastic trajectories can be studied in several ways, most notably by measuring the relevant time scales. As the Fokker-Planck equation is linear, the time evolution of the probability distribution can be understood as the superposition of several eigenmodes associated to nonpositive eigenvalues, all decaying in time with the exception of the first mode that corresponds to the stationary solution. Now, if the first nontrivial (nonzero) eigenvalue λ_1 is separated from the rest and the noise is strong enough, the long term behavior is going to be dominated by the timescale $-1/\lambda_1$. This approach has been used by [24] and many other works, where the effect of the time correlation of the noise has been examined.

Although the expansion (22) can easily be used for posing an eigenvalue problem, here we wanted to answer a more concrete question: how long does it take for the stochastic system to jump from UR to LR (or the other way around)? This question can be posed as a first exit time problem. Such problems have been abundantly explored in the literature by exploiting special properties of the model systems under study (good reviews of colored-noise and exit time problem are [20,26]). Here in this article we follow the more general approach (described in textbooks such as Gardiner's ([27] Sect. 5.4)) and take advantage of the expansion into a complete set to study the dependence of the time correlation of the noise on the exit time.

For this purpose we define a subdomain $R \subset \Omega_2$ that contains the deterministic fixed point UR. For the lower boundary of R one should choose the boundary of the basin of attraction of UR (separatrix). Here we take a simpler option and choose a straight segment that passes through the origin and the unstable fixed point, as depicted in Figure 6. The boundary of the region R is made

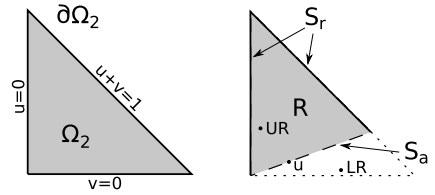

Fig. 6. (a) Two dimensional domain of the reduced Fokker-Planck equation (26). The horizontal and the vertical coordinates are u and v respectively, and the corners of the triangle are points $(0,0),(0,1)$ and $(1,0)$. (b) Region used for the exit time problem equation (31). It contains UR and its absorbing boundary passes through the unstable fixed point 'u' of the deterministic dynamics.

up of two parts: $\partial R = S_a \cup S_r$. The boundary that coincides (at least approximately) with the separatrix S_a must be *absorbing*. The remaining boundaries S_r are *reflecting* (as they were for the forward Fokker-Planck equation (18) and its boundary condition (21)).

The probability $G(u,v,\zeta,t)$ of remaining inside R that obeys the *backward* Fokker-Planck equation (the adjoint of Eq. (18)):

$$\begin{aligned}\partial_t G &= \mathcal{L}^\dagger G \\ &= \left[(f_u + \sqrt{D} g_u \zeta)\partial_u G\right] + \left[(f_v + \sqrt{D} g_v \zeta)\partial_v G\right] \\ &\quad - \frac{1}{\tau}\zeta\partial_\zeta G + \frac{1}{2\tau^2}\partial_\zeta^2 G \end{aligned} \tag{30}$$

in the cylindrical domain $R \times \mathbb{R}$. Appropriate boundary conditions for G are:

$$\hat{\mathbf{n}} \cdot \nabla G = 0 \text{ in } S_r, \text{ and } G = 0 \text{ in } S_a,$$

and initial condition:

$$G(u,v,\zeta,0) = 1 \text{ for } (u,v) \text{ inside } R \text{ and } \zeta \in \mathbb{R}.$$

For the function G we use a similar expansion to equation (22):

$$G(u,v,\zeta,t) = \theta_0^{-1}(\zeta) \sum_{\ell=0}^{\infty} \varphi_\ell(u,v,t)\theta_\ell(\zeta)$$

that after being replaced in equation (30) leads to the following set of equations for $\varphi_\ell(u,v,t)$:

$$\begin{aligned}\partial_t \varphi_\ell &= (f_u\partial_u + f_v\partial_v)\varphi_\ell - \frac{\ell}{\tau}\varphi_\ell \\ &\quad - \sqrt{\frac{D}{8\tau}}(g_u\partial_u + g_v\partial_v)\left(\sqrt{\ell+1}\varphi_{\ell+1} + \sqrt{\ell}\varphi_{\ell-1}\right), \\ &\quad \text{in } R \text{ for } \ell = 0,1,2,\ldots \end{aligned} \tag{31}$$

with boundary conditions:

$$\hat{\mathbf{n}} \cdot \nabla \varphi_\ell = 0 \text{ in } S_r, \text{ and } \varphi_\ell = 0 \text{ in } S_a,$$

and initial condition:

$$\varphi_\ell(u,v,0) = \delta_{\ell,0} \text{ inside } R.$$

Now the mean time required to leave region R starting from point (u,v) and random ζ that follows stationary distribution, can be measured by the function $T(u,v)$ that can be obtained from G:

$$\begin{aligned} T(u,v) &= \int_0^\infty \int_{-\infty}^\infty G(u,v,\zeta,t)\,\theta_0^2(\zeta)\,d\zeta\,dt \\ &= \int_0^\infty \varphi_0(u,v,t)\,dt. \end{aligned} \tag{32}$$

A similar approach could be used for the basin of attraction of LR. In the next section we will compute the evolution of the set φ_ℓ by the Euler method for a reasonably long time, and then integrate in time to compute the mean exit time $T(u,v)$.

5 Numerical results

A complete treatment of the evolution equation for the set of equations (26) and the set of equations (31) (associated to the forward and backward Fokker-Planck equations respectively) can be obtained using the finite element method (FEM). Some of the advantages of FEM compared with finite differences, for this specific problem are: more sophisticated approach to function (Sobolev) spaces; greater control of the approximations; better treatment of complicated geometries; and easier handling of boundary conditions. Another benefit of FEM is the possibility of using adaptive refinement of the mesh as the solution becomes more localized [28].

The FEM solves the associated weak form of the partial differential equations. In this work we use Freefem++, a general-purpose FEM software developed by Frédéric Hecht from Université Pierre et Marie Curie, Paris.

For most of the computations three layers were enough ($\ell = 0,1,2$), because most of the 'energy' is contained in the zero ($\ell = 0$) layer. For Y_0 inside the hysteresis range and small noise, the stationary probability $W(u,v) = \phi_0$ gets the expected bimodal shape and becomes concentrated along a narrow region in phase space i.e. the slow manifold (used in [11,13,15]). As we will see, this dimensionality reduction is not true for stronger or more strongly correlated noise.

Using this expansion approach we can predict how changes in parameters $Y_0, \Delta Y, \tau$ will affect the shape of the probability distribution. For instance switching from bimodal to monomodal distribution by increasing τ. In Figures 7a–7d we show the stationary distribution $W(u,v)$ for four sets of parameters. As larger values of τ are considered, the distribution becomes broader and spreads away from the slow manifold present in Figures 7a and 7b. This qualitative change can be understood in the more general framework of colored-noise effects [17].

Figure 8 shows mean exit time $T(u,v)$. For other values of τ the shape of the contour curves remains similar although the values change.

Figures 9a and 9b show the behavior of the first exit time evaluated at UR fixed point $T(\text{UR})$, for different values of the noise correlation time τ. Ranges of τ in both

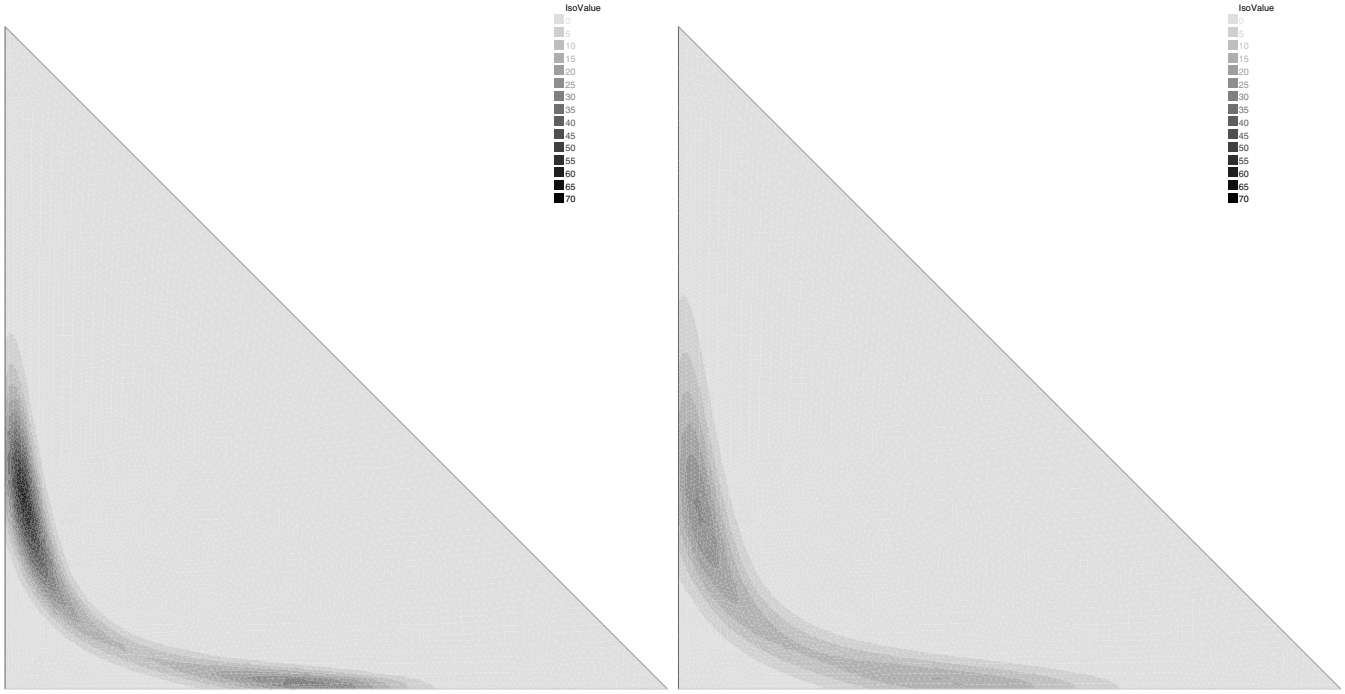

(a)

(b)

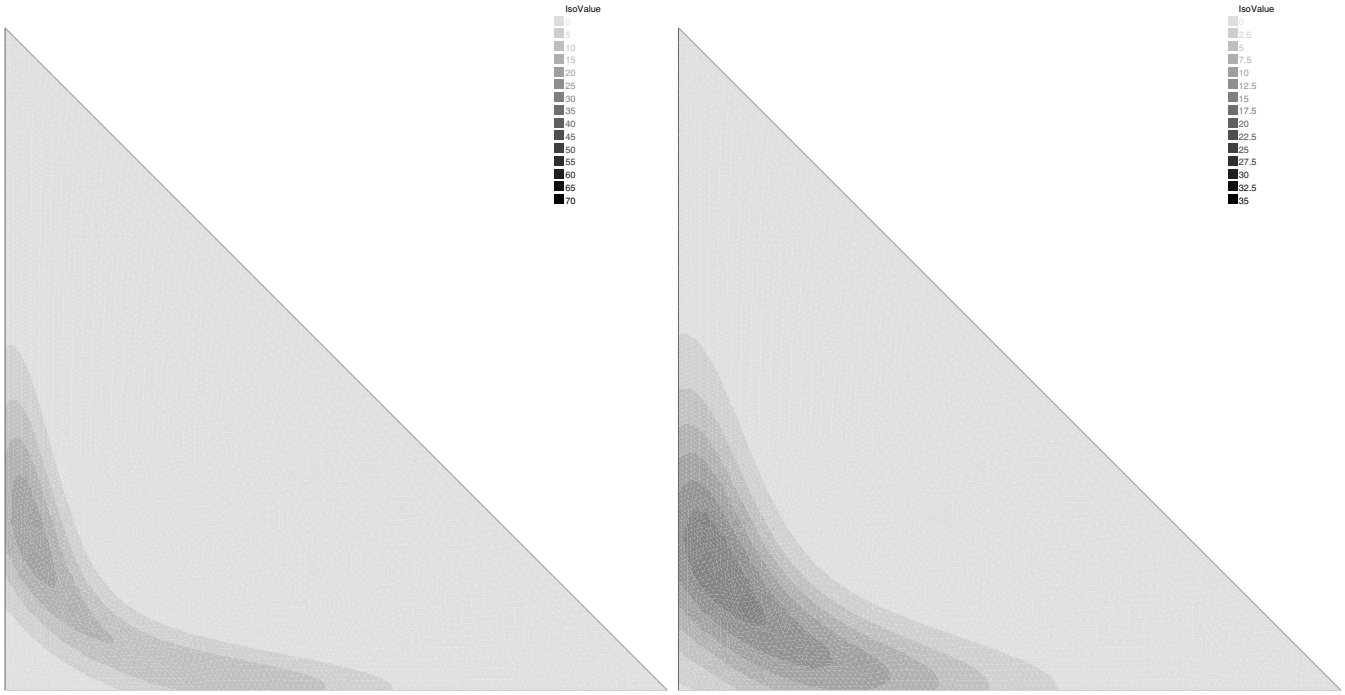

(c)

(d)

Fig. 7. Stationary probability distribution $W(u, v)$ for four different situations: (a) $\tau = 20$; (b) $\tau = 50$; (c) $\tau = 100$; and (d) $\tau = 200$. Other parameters $Y_0 = 0.094, \Delta Y = 0.08$ were held constant. Here the horizontal and the vertical coordinates are u and v respectively, and the corners of the triangle are the points $(0, 0), (0, 1)$ and $(1, 0)$. As τ becomes larger the distribution becomes wider and monomodal, and the one-dimensional slow manifold disappears.

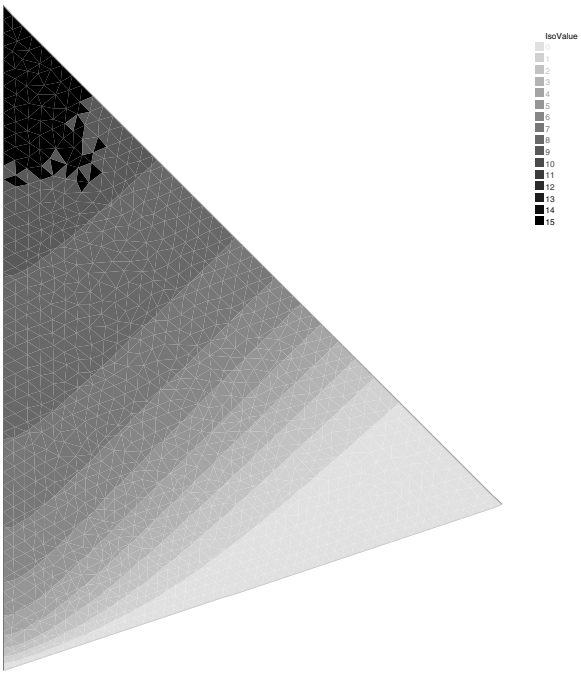

Fig. 8. Mean exit time $T(u, v)$ for $Y_0 = 0.094$, $\Delta Y = 0.08$, $\tau = 100$. The domain of integration R contains the point UR and is described in Figure 6. For other parameters the contour curves of $T(u, v)$ look qualitatively similar.

figures were selected so significative variations in $T(UR)$ were observed. When τ is increased for a given value of ΔY, the value of $T(UR)$ grows and sets into a trend of linear growth with a slope approximately equal to one, as depicted in Figure 9a (see also [29]). This behavior is quite similar to what we could expect from the quasi-static model, that predicted (see Eq. (12)) a linear growth of $T(UR)$.

Now τ has an effect on the effective noise intensity D (Eq. (7)). When τ is increased and ΔY is adjusted so D is kept constant, we see in Figure 9b how the exit time $T(UR)$ actually decreases towards a limiting value. This last result should be compared for instance with eigenvalue computations such as [24] and the results of approximate one-dimensional Fokker-Planck equations [26], that predict (at least) exponential growth of the exit time with τ, for constant values of the noise intensity D. Our conjecture is that increasing values of τ allows the system to explore wider areas of the two-dimensional phase space, as shown in Figures 7c and 7d, that may explain a faster exit from the UR basin of attraction.

6 Conclusions and outlook

Surface reactions are usually affected by the noise that comes from the environment or from impurities. Some of the properties of the noise have a direct incidence on the statistics of the reaction rate, both for transient and stationary behavior.

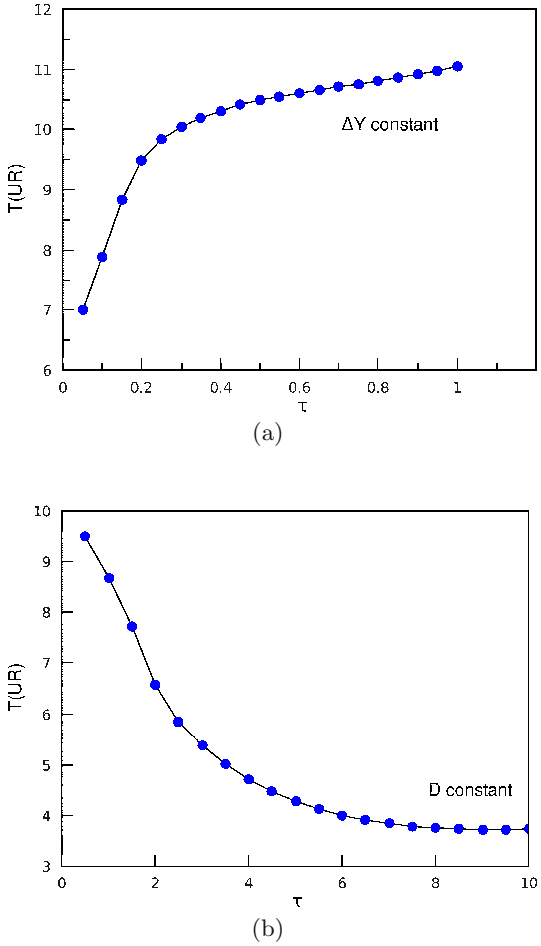

Fig. 9. (Color online) First exit times T evaluated at UR point for different values of τ. (a) When ΔY is kept fixed, the exit time $T(UR)$ grows linearly. (b) When D is kept fixed (and ΔY adjusted accordingly) the exit time decreases towards a limiting value.

In particular we considered here the finite correlation time of the noise. Several theories provide approximations for the probability distribution and the relevant timescales, but for this specific surface reaction model these methods do not work when the noise is strong or when the time correlation is large.

Here we used a discrete time Markov chain and a Ornstein-Uhlenbeck process to compute relevant quantities that describe stochastic behavior. The effects of the Ornstein-Uhlenbeck noise can be analyzed using both forward and backward Fokker-Planck equations, that can be further simplified by an expansion into a complete set in terms of Finite Elements. This approach captures genuine colored-noise effects: changes in the shape of the probability distribution (bimodal and monomodal) as well as in the transition times.

A few words are due about transition times computed by the two methods. On the one hand, the Markov chain, which is good for piecewise-constant noise with long windows, predicts a linear growth of transition time with

correlation time, when the amplitude of the fluctuations is held fixed. On the other hand, Ornstein-Uhlenbeck noise, which is based on very different assumptions and is only a good approximation for moderate correlation times, shows also a linear trend for the transition time. These two approaches seem to be complementary, and a more complete crossover picture should be elaborated.

The approaches used here should be generalizable to other surface reactions. Another interesting example is the CO oxidation on Platinum(110) [1,2,10]. Its deterministic bifurcations are a lot richer than those of Ir(111), exhibiting many more types of bifurcations: Hopf, canard, saddle-node, sniper, etc., so we expect that it will show interesting noise-induced transitions, that can be investigated using either the discrete time Markov chain or the expansion into a complete set used in this work.

This work was supported by an International Cooperation Grant between Germany (DFG Project WE 4100/3) and Chile (Conicyt Project 079-2009): "Effects of large noise in the CO oxidation on Iridium(111) surfaces within the bistable regime". JC was also supported by Universidad de los Andes Grant (Project FAI ING-002-09).

References

1. K. Krischer, M. Eiswirth, G. Ertl, J. Chem. Phys. **96**, 9161 (1992)
2. K. Krischer, M. Eiswirth, G. Ertl, J. Chem. Phys. **97**, 307 (1992)
3. S. Jakubith, H. Rotermund, W. Engel, A. von Oertzen, G. Ertl, Phys. Rev. Lett. **65**, 3013 (1990)
4. J. Cisternas, P. Holmes, I. Kevrekidis, X. Li, J. Chem. Phys. **118**, 3312 (2003)
5. S. Wehner, F. Baumann, J. Küppers, Chem. Phys. Lett. **370**, 126 (2003)
6. Y. Hayase, S. Wehner, J. Küppers, H. Brand, Phys. Rev. E **69**, 021609 (2004)
7. S. Wehner, P. Hoffmann, D. Schmeisser, H. Brand, J. Küppers, Phys. Rev. Lett. **95**, 038301 (2005)
8. M. Pineda, R. Imbihl, L. Schimansky-Geier, C. Zülicke, J. Chem. Phys. **124**, 044701 (2006)
9. M. Pineda, L. Schimansky-Geier, R. Imbihl, Phys. Rev. E **75**, 061107 (2007)
10. P. Bodega, S. Alonso, H. Rotermund, J. Chem. Phys. **130**, 1 (2009)
11. M. Pineda, R. Toral, J. Chem. Phys. **130**, 124704 (2009)
12. S. Wehner, S. Karpitschka, Y. Burkov, D. Schmeisser, J. Küppers, H. Brand, Physica D **239**, 746 (2010)
13. J. Cisternas, D. Escaff, O. Descalzi, S. Wehner, Int. J. Bif. Chaos **19**, 3461 (2009)
14. F. De la Rubia, J. García-Sanz, M. Velarde, Surf. Sci. **143**, 1 (1984)
15. J. Cisternas, D. Escaff, O. Descalzi, S. Wehner, Int. J. Bif. Chaos **20**, 243 (2010)
16. R. Stratonovich, *Theory of Random Noise* (Gordon and Breach, New York, 1963)
17. W. Horsthemke, R. Lefever, *Noise Induced Transitions: Theory and Applications in Physics, Chemistry, and Biology* (Springer, Berlin, 1984)
18. P. Jung, P. Hänggi, Phys. Rev. A **35**, 4464 (1987)
19. H. Malchow, L. Shimansky-Geier, *Noise and Diffusion in Bistable Nonequilibrium Systems* (B.G. Teubner Verlagsgesellschaft, Berlin, 1985)
20. P. Hänggi, P. Jung, in *Advances in Chemical Systems*, edited by I. Prigogine, S. Rice (John Wiley & Sons, New York, 1995), Vol. LXXXIX
21. T. Engel, G. Ertl, J. Chem. Phys. **69**, 1267 (1978)
22. T. Engel, G. Ertl, Adv. Catal. **28**, 1 (1979)
23. S. Wehner, Int. J. Bif. Chaos **19**, 2637 (2009)
24. T. Leiber, F. Marchesoni, H. Risken, Phys. Rev. Lett. **59**, 1381 (1987)
25. H. Risken, *The Fokker-Planck Equation: Methods of Solutions and Applications* (Springer, Berlin, 1989)
26. K. Lindenberg, B. West, J. Masoliver, First passage time problems for non-Markovian processes, in *Noise in nonlinear dynamical systems*, edited by F. Moss, P. McClintock (Cambridge University Press, Cambridge, 1989), Vol. 1, Chap. 4
27. C.W. Gardiner, *Handbook of Stochastic Methods for Physics, Chemistry and the Natural Sciences* (Springer, Berlin, 1983)
28. L. Ferm, P. Lötstedt, P. Sjöberg, Bit Numerical Mathematics **46**, 61 (2006)
29. A. Hernández-Machado, M.S. Miguel, J. Sancho, Phys. Rev. A **29**, 3388 (1984)